Int J Adv Manuf Technol (2015) 79:705–716
DOI 10.1007/s00170-015-6844-5

ORIGINAL ARTICLE

Experimental research of milling force and surface quality for TC4 titanium alloy of micro-milling

Haitao Liu · Yazhou Sun · Yanquan Geng · Debin Shan

Received: 3 July 2014 / Accepted: 27 January 2015 / Published online: 14 February 2015

Abstract Due to its good mechanical and chemical property, titanium alloy is widely used in high-tech industries such as aerospace, biomedical engineering, etc. Utilizing micro-milling to fabricate titanium alloy parts, good surface geometric appearance can be obtained. The dynamic behaviors of milling force and surface quality in micro-milling process of titanium alloy should be investigated. Considering the effect of tool runout, the paper established a mathematical model to calculate the uncut thickness and to describe the dynamic behavior of micro-milling force including the combined influences of tool runout, minimum uncut thickness, and edge plowing. The correctness and applicability of the presented model was also verified from the perspective of micro-milling force experiment and finite element analysis. Meanwhile, experimental results indicated that the surface quality of machined surface is prone to the influence of burrs and residual chips. In the micro-milling process for titanium alloy, a smaller feed per tooth and tool material that is not easy to stick to titanium alloy are preferred, while cooling is necessary if a machined surface with better surface quality is looked forward to.

Keywords Micro-milling · Tool runout · Surface damage · Burr

1 Introduction

Thanks to its light weight, high strength, strong corrosion resistance, and other characteristics, titanium alloy has been widely applied in many fields, such as aerospace structures and medical implant. To improve the biocompatibility of medical implants, consisted of titanium alloy, the surface could be modified with specific functional microstructures. Employing micro-milling to process titanium alloy medical implants parts, a good three-dimensional geometric surface shape can be obtained. Therefore, the milling force and surface quality obtained need to be studied. A large number of scholars have focused the mathematical model used to characterize the dynamic behavior of milling force and to describe the quality of machined surface. Vogler et al. [1, 2] introduced the effect of workpiece microstructure into the mechanical model for the milling tool, explored the effect of minimum uncut thickness, and established the slip-line field model to make an accurate prediction on the plowing force. Jun et al. [3] analyzed the effect of tool vibration caused by dynamic cutting load and improved micro-milling force model, ignoring the spiral angle of flat milling tool. Waldorf [4] proposed a plowing force model in the sliding area and processed 6061 aluminum alloy by using tools with different edge radii to analyze the difference of the milling force. Kim et al. [5] put forward a chip formation model for micro-milling and found that there was some interruption trait at a smaller feed velocity during milling. Kang [6] presented a micro-end milling analytical mechanical model and predicted the milling force when the side faces of tool made contact with workpiece. Bissacco [7] described the influence of tool radius and chip flowing angle on the milling process. Malekian [8] studied a micro-milling force mechanical model consisted of plowing force, spindle jump, and elastic recovery.

In conventional milling process, the defects and burrs on machined surface can be eliminated by posttreatment, but it is quite difficult in the micro-milling process for the size limitation of components. How to obtain a good surface by one process becomes an issue that is urgently solved. Different machining procedures, workpiece shapes, formation

H. Liu · Y. Sun (✉) · Y. Geng · D. Shan
School of Mechanical Engineering, Harbin Institute of Technology, P.O. 422, No. 92, West DaZhi Street, Nangang District, Harbin 150001, China
e-mail: sunyzhit@163.com

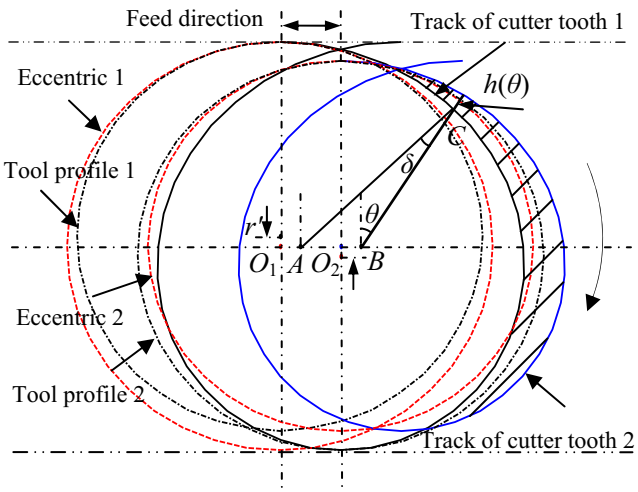

Fig. 1 Edge trochoid schematic diagram considering the effect of tool runout

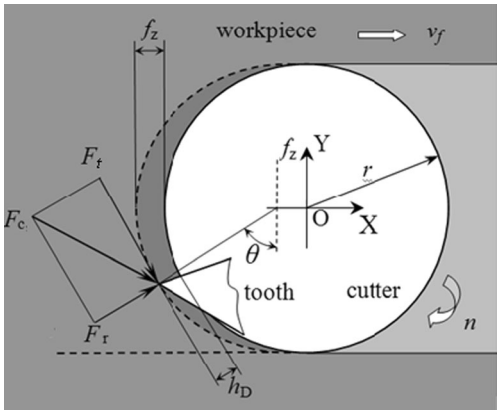

Fig. 3 Rotary cutting force model

mechanism, and material properties will induce the formation of different burrs [9]; the description focused on conventional-size burrs should be conducted based on the causes of burr formation. Nowadays four kinds of burrs are introduced as follows: Poisson burr, reversal burr, tear burr, and cutting out burr. Schueler [10] studied the burr formation at different feed velocities using flat milling tool during the processing of titanium alloys. Vogler et al. [11] analyzed the effect of burrs on surface quality with different tools. Min et al. [12] demonstrated the effect of down-milling and up-milling on surface quality under different process parameters and found that the favorable feed direction of milling had a great effect on surface roughness at slow speed. Liu et al. [13] conducted the milling process of glass materials and verified the influence of milling parameters on surface roughness.

Despite of pioneering researches on conventional cutting processing of titanium alloy, few scholars focused on the micro-milling of titanium alloy [14–16]. Lei et al. [17] utilized the rotary-driven tool to process titanium alloy at high speed and found it could effectively improve the life of the tool. Wang [18] studied the milling force and tool wear mechanism, by using cubic boron nitride tool to process titanium alloy at high speed. Ribeiro [19] optimized the process parameters of titanium alloy. Zhang [20] analyzed the dynamic behaviors of milling force and heat in the milling process of titanium alloy and obtained the feasible milling parameter. Yang [21] developed a three-dimensional finite element model of titanium alloy TC4 according to the two-flute cutter inclined angle cutting theoretical model and simulated the force in the milling process. Schueler et al. [10] utilized micro-radius milling tool to process two kinds of titanium alloys and obtained the

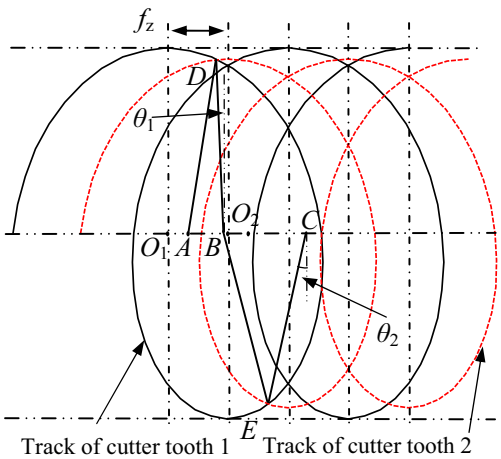

Fig. 2 Calculation diagram of cutting angles considering tool runout

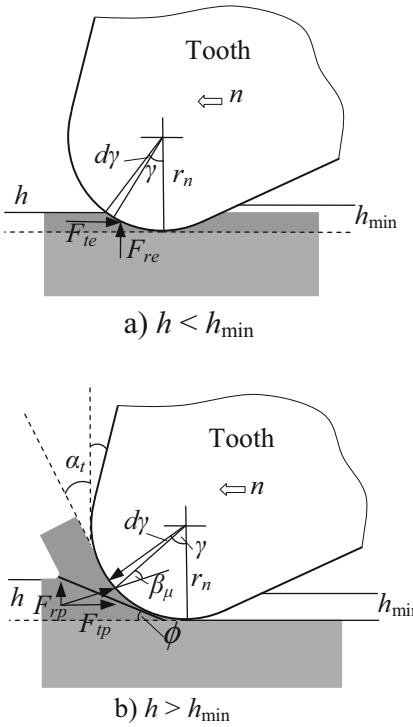

Fig. 4 Micro-cutting force analysis model. **a** $h < h_{min}$. **b** $h > h_{min}$

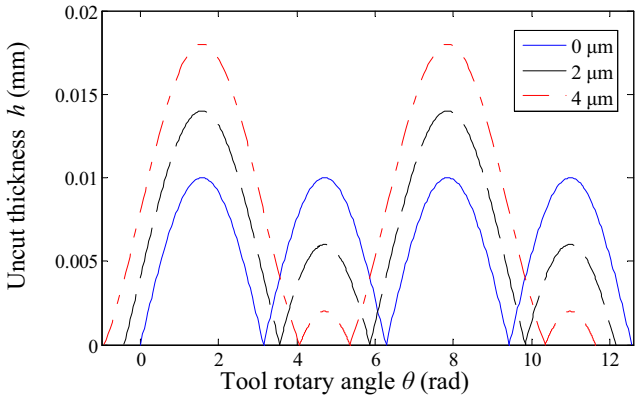

a) feed per tooth f_z =10μm

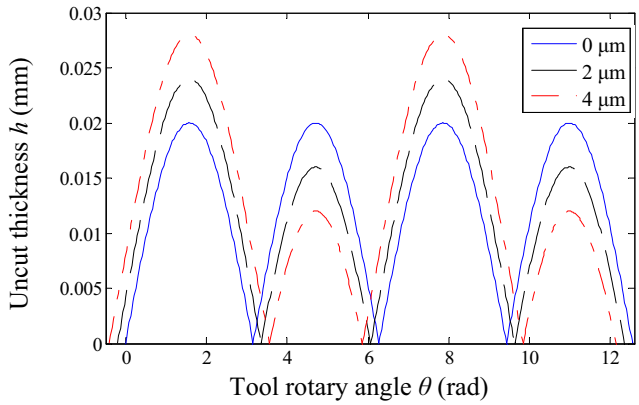

b) feed per tooth f_z =20μm

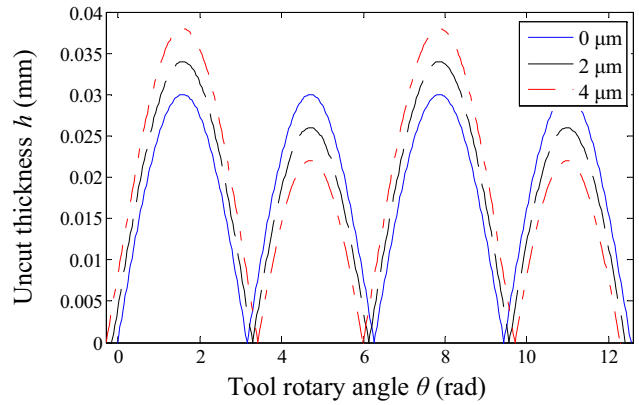

c) feed per tooth f_z =30μm

Fig. 5 The influence of tool runout on uncut thickness. **a** feed per tooth f_z=10 μm. **b** feed per tooth f_z=20 μm. **c** feed per tooth f_z=30 μm

large area of surface microstructures and compared the burrs. Özel et al. [22] studied the influence of micro-tools coated by CBN on the surface roughness of titanium alloy machined surface, burr formation, and tool wear through experiment and finite element simulation. Özel et al. [23] conducted the multi-objective optimization for the micro-milling parameters of Ti-6Al-4V material in order to improve the surface

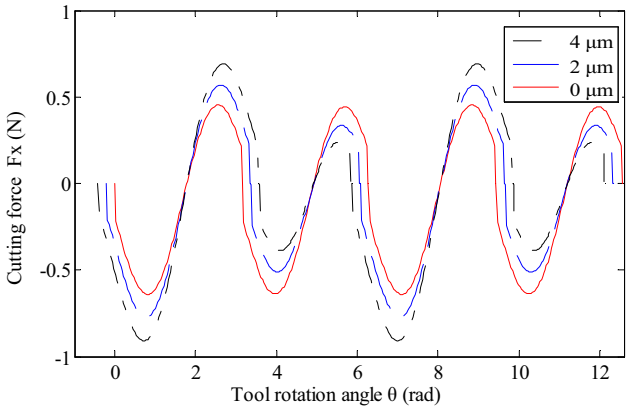

a) Cutting force in the feeding direction F_x

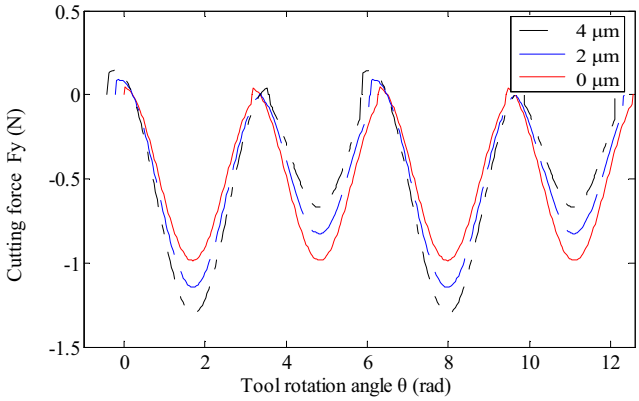

b) Cutting force in the vertical direction of feeding F_y

Fig. 6 The influence of tool runout on cutting force. **a** Cutting force in the feeding direction F_x. **b** Cutting force in the vertical direction of feeding F_y

roughness and remove or reduce the formation of burrs. Afazov et al. [24] studied the influence of tool runout on uncut thickness, but that of the cutting angle was ignored.

Tool clamping error will lead to the misalignment between the tool axis and spindle rotary axis, which is of significance on the micro-milling process. The role that tool runout played in the cutting process should not be ignored for the tiny dosage

Fig. 7 Experiment system

Table 1 Processing parameters

Tool parameters			Micro-milling parameters		
Tool radius	Helical angle	Edge length	Spindle speed	Feed per tooth	Cutting depth
0.5 mm	30°	1.5 mm	200,00 r/min	5 μm/z	10 μm

of micro-milling. Tool runout could induce the difference of uncut thickness between two-flute cutters, which will lead to the deviation of milling force exerted on two cutting edges, and even affect the life of cutting tool, machining precision, as well as the surface quality. However, previous theoretical model ignored the influences of tool runout and cutting angle on the micro-milling, while few researches focused on the effect of chip on the formation of surface defects. The paper proposed a predictive mathematical model of micro-milling force, which takes the combined effect of tool runout and tool edge radius into account and presented the experimental results of the micro-milling surface roughness and defects.

2 Mathematical modeling of micro-milling force

2.1 Calculation of instantaneous uncut thickness

Generally, micro cutting tool possesses a couple of cutting edges. This paper proposed a theoretical model to describe the machining process using two-flute cutter milling tool. In order to accurately demonstrate the milling force and roughness, the influence of tool runout is considered in the modeling process. As shown in Fig. 1, the cycloid trajectory diagram of two-flute cutter milling introduces the effect of tool runout, where r, r' denote the edge radius of the tool runout, respectively, and $(r-r')$ and $(r+r')$ represent the gyration radius of two cutting edges separately. The tool runout causes the change of instantaneous uncut thickness $h(\theta)$ and then leads to the variation of cutting force in the micro-milling process.

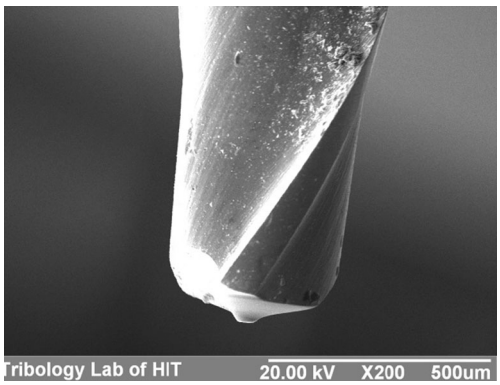

Fig. 8 SEM photograph of micro-milling tool with two-flute

Based on the schematic diagram above, the uncut thickness under different tool runout could be calculated using Eq. 1,

$$h(\theta)=\begin{cases} r-r'-\dfrac{\cos\left(\theta+\dfrac{\pi f_z\cos\theta}{\pi(r+r')+f_z\cos\theta}\right)}{\cos\theta}(r+r') & \left(\theta_{en}\le\theta\le\theta_{ex}\quad\theta\neq\dfrac{\pi}{2}\right) \\ f_z-2r' & (\theta=\pi/2) \end{cases} \tag{1}$$

where f_z *is* the feed per tooth, θ is tool rotation angle, and θ_{en} and θ_{ex} are entrance and exit angles of cutting, respectively, which denote the angles between tooth radius and vertical direction, when the cutting edge's entrance and exit of the material is performed. Herein, a negative value means an angle in the fourth quadrant.

2.2 Cutting angles

Unlike conventional milling process, the mathematical model that could be applied to describe the dynamic behavior of milling force emerging in micro-milling process is susceptible to the tool geometry and cutting conditions. Herein, the hypothesis that the entrance angle is 0°and the exit angle is 180° is no longer valid now. The calculation of cutting angles could be expressed using the diagram in Fig. 2.

According to Fig. 2, θ_1、 and θ_2 can be calculated by Eqs. 2, 3, 4, and 5 below:

$$\frac{\cos\theta_1}{r+r'}=\frac{\sin\left(\left(f_z-\overline{AB}\right)\pi/f_z\right)}{\overline{AB}} \tag{2}$$

$$\frac{\cos\theta_1}{r+r'}=\frac{\cos\left(\left(f_z-\overline{AB}\right)\pi/f_z-\theta_1\right)}{r-r'} \tag{3}$$

$$\frac{\cos\theta_2}{r+r'}=\frac{\sin\left(\left(\overline{BC}-f_z\right)\pi/f_z\right)}{\overline{BC}} \tag{4}$$

$$\frac{\cos\theta_2}{r+r'}=\frac{\cos\left(\left(\overline{BC}-f_z\right)\pi/f_z-\theta_2\right)}{r-r'} \tag{5}$$

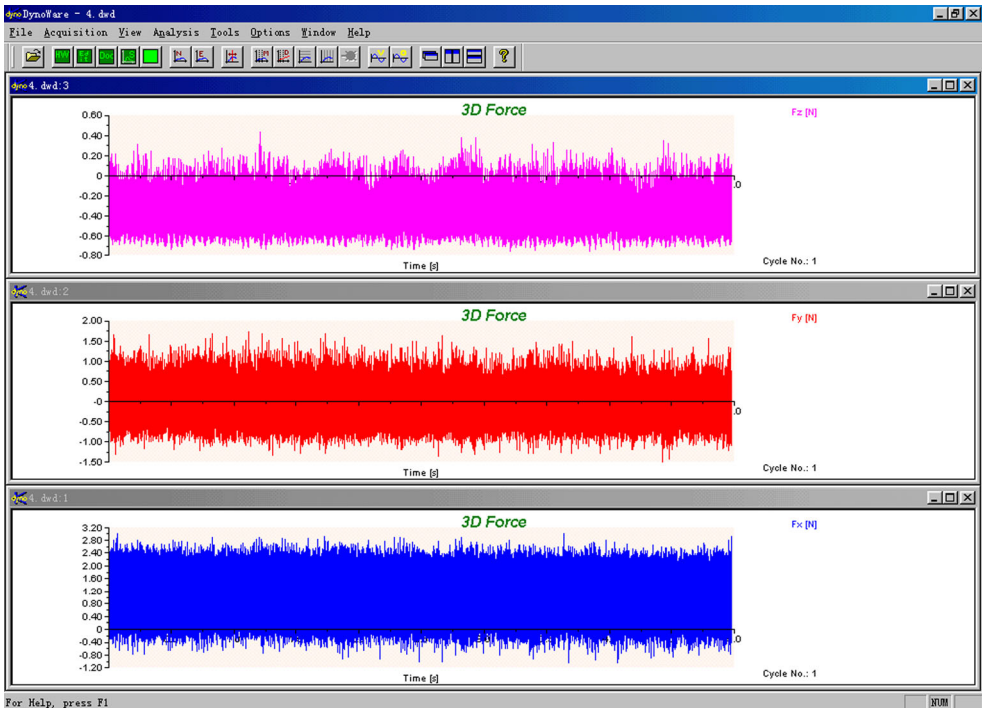

Fig. 9 Initial micro-milling force versus time

θ_{en}、 and θ_{ex} can be expressed using Eq. 6

$$\theta_{en} = -\theta_1 \qquad \theta_{ex} = \pi + \theta_2 \tag{6}$$

2.3 Calculation of micro-milling force

A mechanistic model, considering the combined effect of tool runout and minimum chip thickness, is presented to predict the dynamic behavior of milling force in the micro-milling process, as is shown in Fig. 3, where h is the uncut thickness and F_{te}、 and F_{re} denote horizontal and vertical forces, respectively. Furthermore, an orthogonal cutting model can be developed if the rotary cutting force model is unfolded along the tool's tangential line.

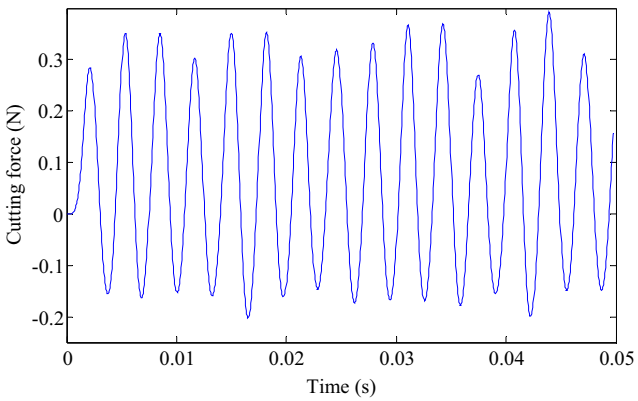

Fig. 10 Filtered micro-filling force versus time

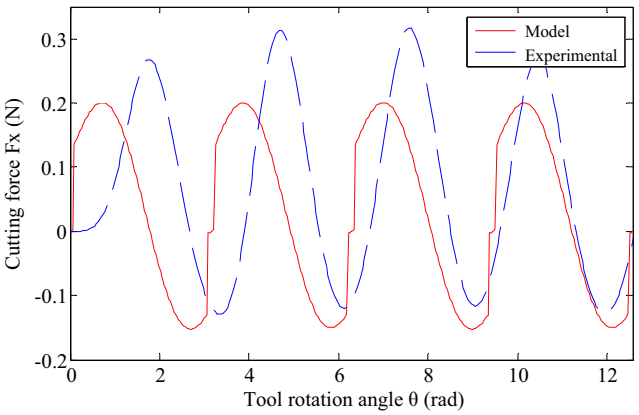

a) Cutting force in the feeding direction F_x

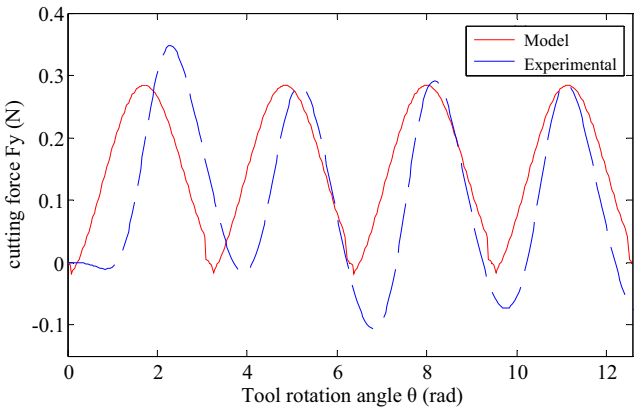

b) Cutting force in the vertical direction of feeding F_y

Fig. 11 Comparison of theoretical and experimental cutting forces. **a** Cutting force in the feeding direction F_x. **b** Cutting force in the vertical direction of feeding F_y

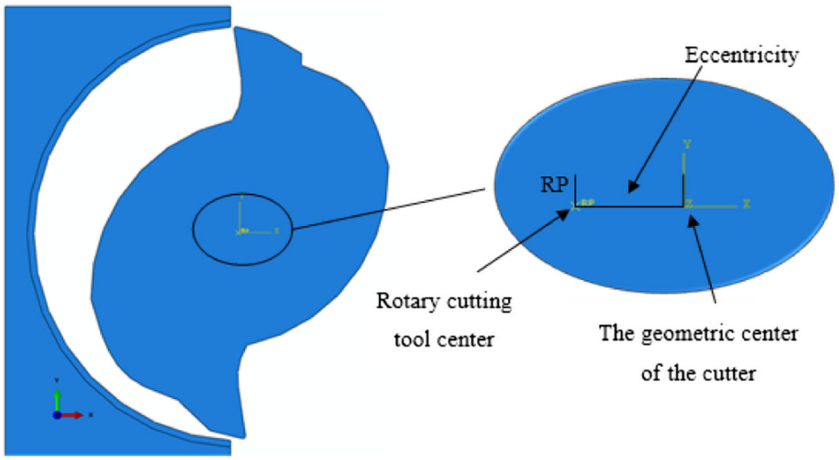

Fig. 12 Tool runout model

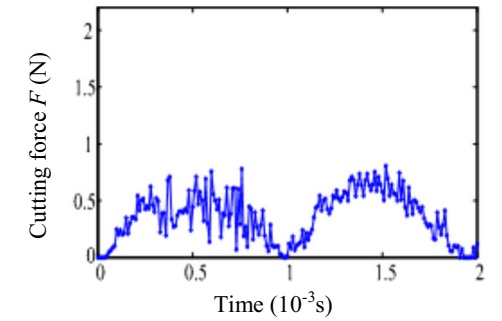

a) Tool run-out 0μm

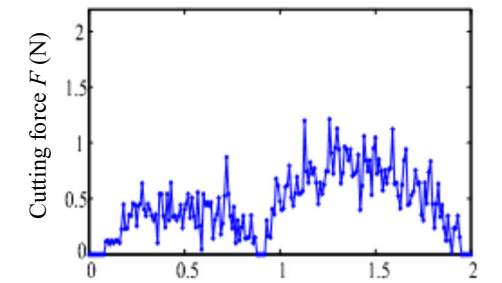

b) Tool run-out 2μm

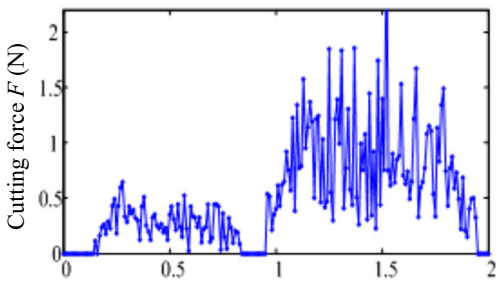

c) Tool run-out 4μm

Fig. 13 Cutting forces under different eccentricities. **a** Tool runout 0 μm. **b** Tool runout 2 μm. **c** Tool runout 4 μm

When the chip thickness, h, decreases to less than the minimum chip thickness, $h_{\min}$, the plastic deformation occurs, due to the coupled impact of tool's extrusion and friction. Meanwhile, when the tool goes through the workpiece, the material is plowed, but no chip was formed. One part of the plowed material occurs at elastic recovery, which can be indicated in Fig. 4a.

The cutting forces can be calculated by following Eq. 7:

$$\begin{aligned} F_{te} &= \int_0^{\arccos((r_n-h)/r_n)} b(\sigma_e r_n \sin\gamma + \mu\sigma_e r_n \cos\gamma)d\gamma \\ F_{re} &= \int_0^{\arccos((r_n-h)/r_n)} b(\sigma_e r_n \cos\gamma - \mu\sigma_e r_n \sin\gamma)d\gamma \end{aligned} \tag{7}$$

where σ_e, b, μ, and γ represent elastic limit of material, cutting width, friction coefficient, and contact angle, respectively. The Eq. 8 can be acquired from Eq. 7 through integration.

$$\begin{aligned} F_{te} &= b\mu\sigma_e\sqrt{r_n{}^2-(r_n-h)^2} - b\sigma_e(r_n-h) + b\sigma_e r_n \\ F_{re} &= b\sigma_e\sqrt{r_n{}^2-(r_n-h)^2} + b\mu\sigma_e(r_n-h) - b\sigma_e r_n\mu \end{aligned} \tag{8}$$

However, if the uncut thickness h increases to greater than the minimum uncut thickness, that is $h > h_{\min}$ (shown in 3b), the material is removed with the formation of chip while the elastic recovery is assumed to be negligible. Meanwhile, the cutting force should be obtained according to the Eq. 9 considering the effect of the shear zone stress, as follows:

$$\begin{cases} F_{tp} = \dfrac{\tau_c hb\cos(\beta_\mu - \alpha_t)}{\sin\phi\cos(\varphi + \beta_\mu - \alpha_t)} \\ F_{rp} = \dfrac{\tau_c hb\sin(\beta_\mu - \alpha_t)}{\sin\phi\cos(\varphi + \beta_\mu - \alpha_t)} \end{cases} \tag{9}$$

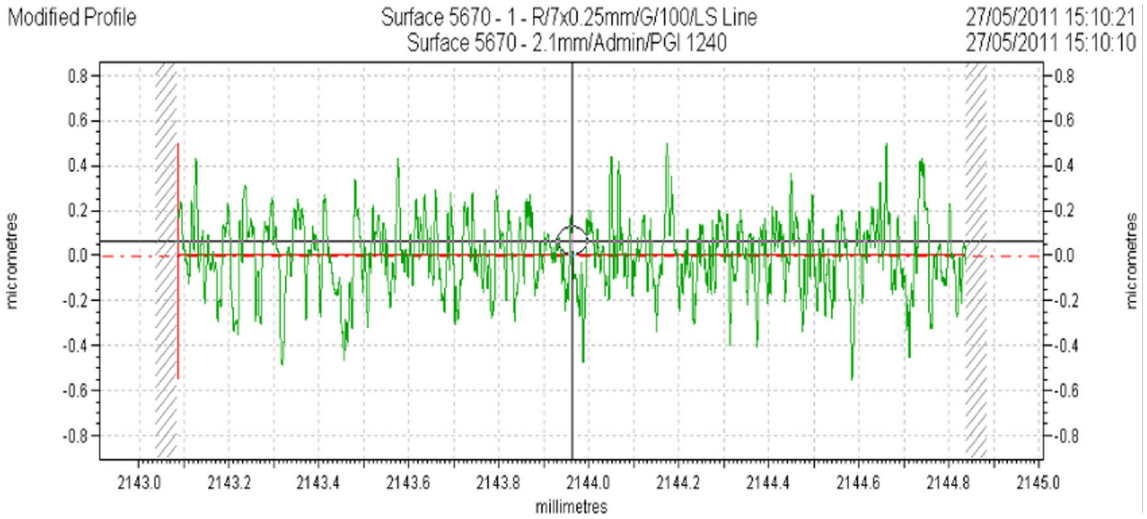

Fig. 14 Machined surface contour

where τ_c and φ represent shear stress and shear angle, respectively.

Besides, tool's edge plowing force in the ductile cutting process was considered and can be expressed by the model proposed by Waldorf [4] (Eq. 10):

$$P_c = \frac{k \cdot b \cdot R}{\sin\eta} \cdot \begin{bmatrix} \cos(2\eta)\cos(\varphi - \gamma' + \eta) - \\ (1 + 2\alpha + 2\gamma' + \sin(2\eta))\sin(\varphi - \gamma' + \eta) \end{bmatrix}$$
$$P_t = \frac{k \cdot b \cdot R}{\sin\eta} \cdot \begin{bmatrix} (1 + 2\alpha + 2\gamma' + \sin(2\eta))\cos(\varphi - \gamma' + \eta) \\ +\cos(2\eta)\sin(\varphi - \gamma' + \eta) \end{bmatrix} \quad (10)$$

And the cutting force could be calculated by Eqs. 11 and 12:

$$\begin{cases} F_t = F_{te} + F_{tp} + P_t \\ F_r = F_{re} + F_{rp} + P_c \end{cases} \quad (11)$$

$$\begin{cases} F_x = -F_t\cos\theta - F_r\sin\theta \\ F_y = F_t\sin\theta - F_r\cos\theta \end{cases} \quad (12)$$

2.4 Model validation

In the micro-milling process, the two blades of the tool will contact with workpiece periodically and the period is equal to the time taking when each blade conducts the cutting of workpiece once. The uncut thickness h and milling force affected by tool runout will vary periodically, as tool rotary angle θ increases, as shown in Figs. 5 and 6, which is obtained in the numerical simulation with by Matlab software.

From the results obtained from Matlab simulations involved above, it can be inferred that tool runout has great influence on uncut thickness and cutting force, due to the tiny feeding in micro-milling process. If the feed per tooth decreases to a critical value, single edge cutting will occur. Therefore, in order to obtain a fine machined surface with good surface quality and less tool wear by micro-milling, the larger tool runout should be avoided.

As shown in Fig. 7, a minitype vertical CNC milling machine was utilized in the micro-milling experiment where the maximum rotary speed of the tool was set to 60,000 r/min, and a three-dimensional dynamometer Kistler was adopted to probe the cutting forces. The process parameters involved in the micro-milling were summarized in Table 1, while the SEM photograph of the micro-milling tool used is shown in Fig. 8.

Figure 9 displays the obtained initial micro-milling force. To eliminate the interference stemming from others, Butterworth filter method was applied and the filtered micro-milling force was shown in Fig. 10, which is consistent with the experimental results.

It can be seen from Fig. 11 that theoretical cutting forces, along the feeding and its vertical direction, agree well with those obtained by the milling experiment, even though the amplitudes are not well matched Note that a complete cycle waveform emerges with each cycle, and the amplitude of the cutting force F_x in positive direction from experiment is about 0.3 N and that in negative direction is about 0.12 N. The cutting force F_y is almost positive, which should be caused by the

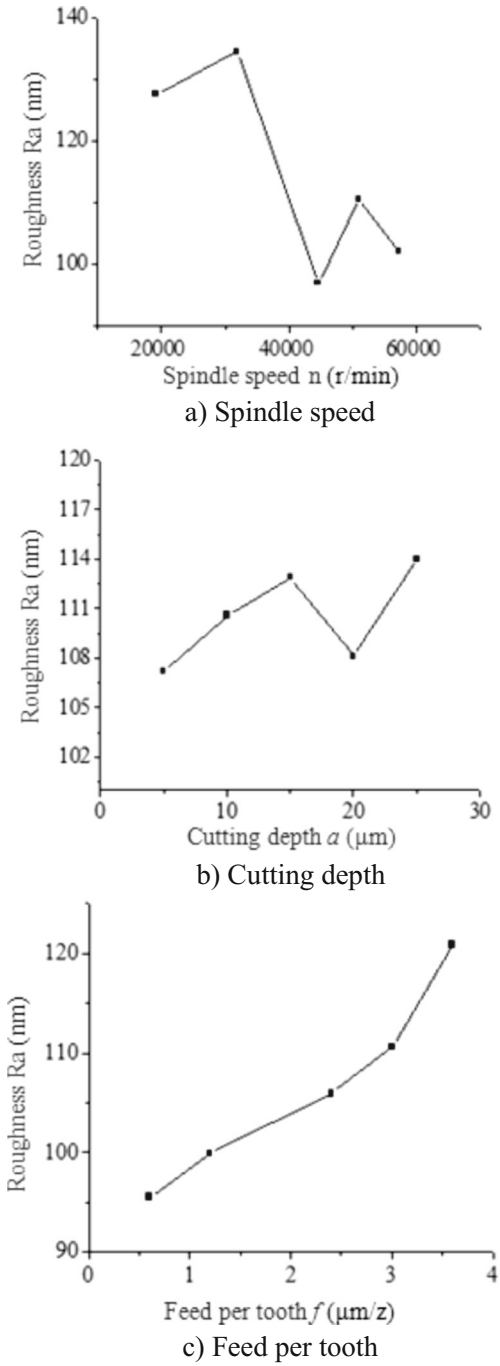

Fig. 15 the effect of spindle speed on surface roughness. **a** Spindle speed. **b** Cutting depth. **c** Feed per tooth

influence of tool deformation or the machining tool errors.

3 Finite element simulations

Figure 12 depicts the finite element model of the tool with runout built by using ABAQUS software, tool's center of gyration was set to be the tool reference point (RP), while the geometric center of tool is fixed at the origin of coordinate system. Herein, the tool runout can be represented by the distance between reference point and the origin of coordinate system. To mimic the specific micro-milling process with runout, tool rotates around RP when it is moved. In order to demonstrate the effect of tool runout on the milling process, the cutting forces including the effect of tool runout are obtained and shown in Fig. 13.

We observe that one of tool edge suffers a smaller force while the other one suffers a larger force when the feeding per tooth is constant, due to the existence of tool runout. Moreover, as the tool runout increases, the difference between the cutting forces increases and tends to grow, and this is in good agreement with results obtained by theoretical predictions.

4 Research on surface topography and burr in micro-milling of titanium alloy

4.1 Surface roughness

Taylor Hobson surface profiler was chosen to measure the roughness of machined surface, and the influence of cutting parameters was examined in the paper. Figure 14 illustrates the surface roughness of 0.1275 μm obtained at the spindle speed of 19,140 r/min, feeding per tooth 3 μm/z, and axial cutting depth 10 μm.

Figure 15 shows the effect of cutting parameters on the surface roughness. Note that surface roughness tends to decrease as the spindle speed increases, but there is almost no change despite the axial depth of cut. Therefore, the axial depth of cut has little effect on the surface roughness of the machined surface, while surface roughness increases with the feed per tooth.

4.2 Surface morphology

Titanium alloy possesses a low thermal conductivity coefficient and high adhesion, and the temperature in the milling process is pretty high, which will have a great influence on the surface quality. Figure 16 indicates the surface morphology and defects on machined surface with groove texture, which is obtained at a spindle speed n=44,580 r/min, at different feeds per tooth, and a cutting depth of 10 μm by using a three-dimensional stereoscopic microscope with super depth of field.

The distance between two cutting traces in Fig. 16 represents that the cutting edge scratches across the machining surface twice. It can be observed that the density of cutting traces is much larger and surface quality

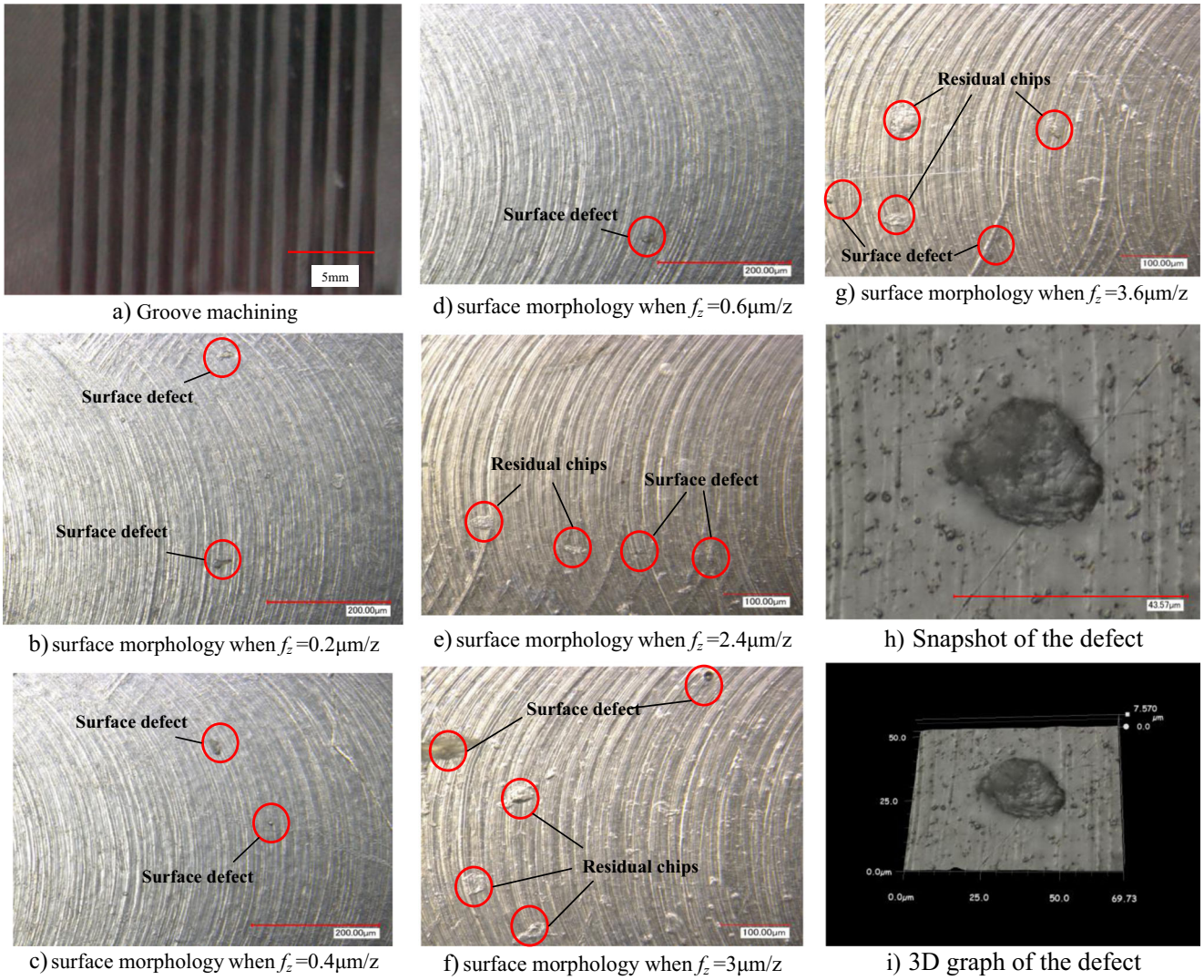

a) Groove machining
d) surface morphology when f_z=0.6μm/z
g) surface morphology when f_z=3.6μm/z
b) surface morphology when f_z=0.2μm/z
e) surface morphology when f_z=2.4μm/z
h) Snapshot of the defect
c) surface morphology when f_z=0.4μm/z
f) surface morphology when f_z=3μm/z
i) 3D graph of the defect

Fig. 16 Surface profile and defects. **a** Groove machining. **b** surface morphology when f_z=0.2 μm/z. **c** surface morphology when f_z=0.4 μm/z. **d** surface morphology when f_z=0.6 μm/z. **e** surface morphology when f_z=2.4 μm/z. **f** surface morphology when f_z=3 μm/z. **g** surface morphology when f_z=3.6 μm/z. **h** Snapshot of the defect. **i** 3D graph of the defect

becomes better when the feed per tooth is in the range of 0.2~0.6 μm/z, while there are more surface defects when the feed per tooth reaches to 2.4~3 μm/z. Figure 16h, i illustrates the enlarged view of surface defects on machined surface, and it can be noted that the defect's height is about 7.5 μm and is pretty large, compared with surface roughness, which has a great influence on the surface quality of the machined surface. Herein, the formation of defects should be attributed to the higher bonding between titanium alloy and tool, or the chips that stick to the tool in the fabrication.

4.3 Residual burrs

In the micro-milling process, the formation of burrs is almost inevitable, which will deteriorate the surface quality. To provide more insight s into the formation mechanism of residual burrs at different feeds per tooth, the microscope with super depth of field was applied and the results were shown in Fig. 17. Burrs located near the entrance edge are much smaller and less than those near the exit side. Meanwhile, it can be found that burrs formed mainly pile up around the groove's edge, which will stick to the machined surface and damage the surface directly; moreover, the number of those tend to be much less if the feeding per tooth is in the range from 0.2 to 0.6 μm/z, although the volume and length of the burrs become larger.

In order to clearly characterize the morphology of fabricated groove texture, the SEM was selected to probe the surface quality of the micro-grooves. As observed from Fig. 18, burrs in the entrance side are

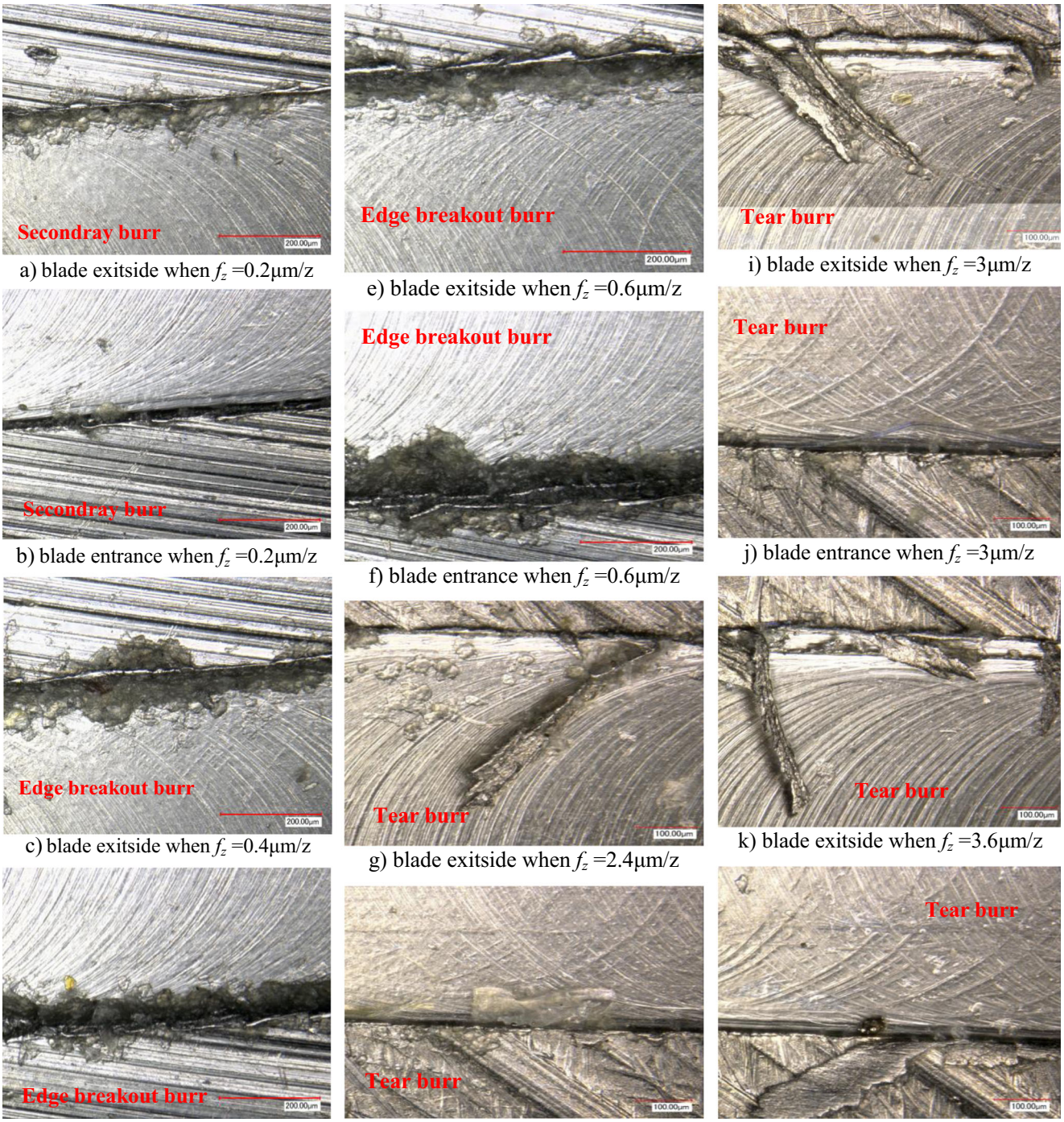

Fig. 17 Residual burrs on machined surface. **a** blade exit side when f_z= 0.2 μm/z. **b** blade entrance when f_z=0.2 μm/z. **c** blade exit side when f_z= 0.4 μm/z. **d** blade entrance when f_z=0.4 μm/z. **e** blade exit side when f_z= 0.6 μm/z. **f** blade entrance when f_z=0.6 μm/z. **g** blade exit side when f_z= 2.4 μm/z. **h** blade entrance when f_z=2.4 μm/z. **i** blade exit side when f_z= 3 μm/z. **j** blade entrance when f_z=3 μm/z. **k** blade exit side when f_z= 3.6 μm/z. **l** blade entrance when f_z=3.6 μm/z

apparently much less than those in the exit side. Furthermore, residual burrs become much larger and are often tear burrs, which agrees well with the experimental results acquired by the microscope with super depth of field.

Some approaches to control the burr formation have been presented, a smaller feed per tooth and a tool material that is not easily sticked to titanium alloy are preferred, while the cooling should be applied in order to decrease the temperature during the milling

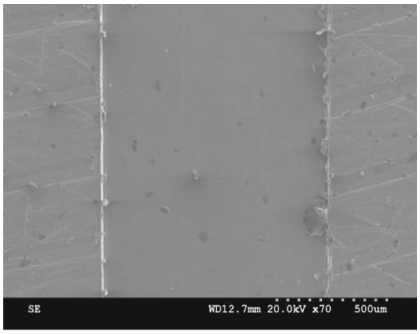

a) n=44580r/min, a_p=10μm, f_z=0.4μm/z micro-groove

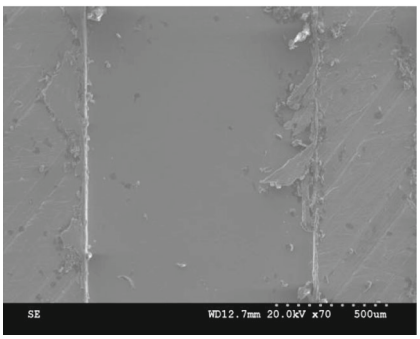

b) n=44580r/min, a_p=10μm, f_z=3μm/z micro-groove

Fig. 18 SEM pictures of micro-grooves. **a** n=44,580 r/min, a_p=10 μm, f_z=0.4 μm/z micro-groove. **b** n=44,580 r/min, a_p=10 μm, f_z=3 μm/z micro-groove

process, which is important for the control of burr formation.

5 Summary

With the objective to characterize the dynamic behavior of cutting forces and describe the influence of factors, such as tool runout, spindle speed, and feed per tooth, on the micro-milling process and surface quality of fabricated surface, some researches were performed in this paper, and the conclusions are organized as follows:

1) Due to tiny feed of the micro-milling process, the tool runout has great influence on uncut thickness and cutting forces. When the feed per tooth decreases to a critical value, single edge cutting occurs. The theoretical cutting forces in feeding direction and its vertical direction are well consistent with those obtained by experiments and finite element analysis, though there are some difference between the amplitudes, which is due to the effect caused by tool's deformation and machine tool error.
2) The surface roughness tends to decrease with the increase of the spindle speed but deteriorate when the feeding per tooth is high, while axial depth has no obvious effect.
3) The low feed per tooth leads to a machined surface with better surface quality, such as fewer defects, and a better texture.
4) The feed per tooth has a great influence on the formation of burrs. Burrs located around the entrance edge are much smaller and less, compared with those near the exit side of milling. A larger feed per tooth tends to induce the formation of bigger burrs, that is tear burrs, which will induce the damage of the machined surface.

Acknowledgments The authors would like to thank the Fundamental Research Funds for the Central Universities (Grant No. HIT. NSRI F.2014055) for providing financial support to this research.

References

1. Vogler M, DeVor R, Kapoor S (2003) Microstructure-level force prediction model for micro-milling of multi-phase materials. J Manuf Sci Eng 125:202–210
2. Vogler M, DeVor R, Kapoor S (2004) On the modeling and analysis of machining performance in micro-end milling, part II, cutting force prediction, ASME. J Manuf Sci Eng 126(4):695–705
3. Jun MBG, Liu X, DeVor RE, Kapoor SG (2006) Investigation of the dynamics of micro end milling—part 1: model development. J Manuf Sci Eng 128:893–900
4. Waldorf DJ, DeVor RE, Kapoor S (1998) A slip-line field for ploughing during orthogonal cutting. J Manuf Sci Eng 120:693–700
5. Kim C, Mayor J (2004) A static model of chip formation in micro-scale milling. J Manuf Sci Eng 126:710–719
6. Kang L, Kim JH, Kang M, Seo Y (2007) A mechanistic model of cutting force in the micro end milling process. J Manuf Sci Eng 187–188:250–255
7. Bissacco G, Hansen H, Slunsky J (2008) Modelling the cutting edge radius size effect for force prediction in micro milling. Manuf Technol 57:113–116
8. Malekian M, Park S, Jun M (2009) Modelling of dynamic micro-milling cutting force. Int J Mach Tools Manuf 49:586–598
9. Gillespie LK, Blotter PT (1976) The formation and properties of machining burrs, transaction of the ASME. J Eng Ind 98:66–74
10. Schueler GM, Engmann J, Marx T, Haberland R, Aurich JC. (2010) Burr formation and surface characteristics in micro-end milling of titanium alloys. Burrs-Analysis, Control and Removal, 129-138
11. Vogler MP, DeVor RE, Kapoor SG (2004) On the modeling and analysis of machining performance in micro-end milling, part I: surface generation. J Manuf Sci Eng 126(4):685–694
12. Min S, Sangermann H, Mertens C, Dornfeld D (2008) A study on initial contact detection for precision micro-mold and surface generation of vertical side walls in micromachining. CIRP Ann Manuf Technol 57(1):109–112
13. Liu HT, Sun YZ (2013) Experimental research of brittle-ductile transition conditions and tool wear for micro milling of glass material. Int J Adv Manuf Technol 68:1901–1909
14. Kitagawa T, Kubo A, Maekawa K (1997) Temperature and wear of cutting tools in high-speed machining of Inconel 718 and TI-6Al-6V-2Sn. Wear 202:142–148
15. Ezugwu EO, Wang ZM (1997) Titanium alloys and their machinability—a review. J Mater Process Technol 68(3):262–274
16. Narutaki N, Murakoshi A (1983) Study on machining of titanium alloys. CIRP Ann 32(1):65–69
17. Lei ST, Liu WJ (2002) High speed machining of titanium alloys using the driven rotary tool. Int J Mach Tools Manuf 42:653–661

18. Wang ZG, Wong YS, Rahman M (2005) High speed milling of titanium alloys using binderless CBN tools. Mach Tools Manuf 45:105–114
19. Ribeiro MV, Moreira MRV, Ferreira JR (2003) Optimization of titanium alloy machining. J Mater Process Technol 458–463:143–144
20. Zhang XH, Xu XX, Chen M, Rong B, Liu G (2011) Cutting parameter optimization based on force and heat constraint in milling TC4 titanium alloy. Key Eng Mater 455:307–312
21. Yong Y, Li CH, Sun J (2010) Three-dimensional numerical simulation of cutting force during milling of titanium alloy Ti6Al4V. J Basic Sci Eng 18(3):493–502
22. Özel T, Thepsonthi T, Ulutan D, Kaftanoğlu B (2011) Experiments and finite element simulations on micro-milling of Ti-6Al-4V alloy with uncoated and CBN coated micro-tools. CIRP Ann Manuf Technol 60(1):85–88
23. Thepsonthi T, Özel T (2012) Multi-objective process optimization for micro-end milling of Ti-6Al-4V titanium alloy. Int J Adv Manuf Technol 63(9–12):903–914
24. Afazov SM, Ratchev SM, Segal J (2010) Modelling and simulation of micro-milling cutting forces. J Mater Process Technol 210:2154–2162